

1 **New insight into the spatiotemporal variability and source apportionments of**
2 **C₁-C₄ alkyl nitrates in Hong Kong**

3 Z.H. Ling^{1,2}, H. Guo^{2*}, I.J. Simpson³, S.M. Saunders⁴, S.H.M. Lam^{4,5}, X.P. Lyu², D.R.
4 Blake³

5 ¹ School of Atmospheric Sciences, Sun Yat-sen University, Guangzhou, China

6 ² Air Quality Studies, Department of Civil and Environmental Engineering, The Hong
7 Kong Polytechnic University, Hong Kong

8 ³ Department of Chemistry, University of California, Irvine, California, USA

9 ⁴ School of Chemistry and Biochemistry, University of Western Australia, Perth,
10 Western Australia, Australia

11 ⁵ Pacific Environment Limited, Perth, Western Australia, Australia

12

13 * Corresponding author. Tel: +852 34003962. Fax: +852 23346389. Email:
14 ceguohai@polyu.edu.hk

15

1 **Abstract**

2 C₁-C₄ alkyl nitrates (RONO₂) were measured concurrently at a mountain site (TMS)
3 and an urban site (TW) at the foot of the same mountain in Hong Kong from
4 September to November 2010. Although the levels of parent hydrocarbons were much
5 lower at TMS ($p < 0.05$), similar alkyl nitrate levels were found at both sites regardless
6 of different elevations of the sites, suggesting different source contributions of alkyl
7 nitrates at the two sites, which was proved by the analysis of photochemical evolution
8 of alkyl nitrates. Prior to using a positive matrix factorization (PMF) model, the data
9 at TW were divided into “meso” and “non-meso” scenarios for the investigation of
10 source apportionments with the influence of mesoscale circulation and regional
11 transport, respectively. Secondary formation was the prominent contributor of alkyl
12 nitrates in the “meso” scenario ($60 \pm 2\%$, 60.2 ± 1.2 pptv), followed by biomass
13 burning and oceanic emissions, while biomass burning and secondary formation made
14 comparable contributions to alkyl nitrates in the “non-meso” scenario, highlighting
15 the strong emissions of biomass burning in the inland Pearl River Delta (PRD) region.
16 On the other hand, alkyl nitrates at TMS were mainly due to the photo-oxidation of
17 parent hydrocarbons at TW when mesoscale circulation, *i.e.*, valley breezes occurred,
18 contributing 52-86% to the levels of alkyl nitrates at TMS. In contrast, regional
19 transport from the inland PRD region made significant contributions to the levels of
20 alkyl nitrates (~58-82%) at TMS in the “non-meso” scenario, resulting in similar
21 levels of alkyl nitrates observed at the two sites. The simulation of secondary
22 formation pathways using a photochemical box model found that the reaction of alkyl
23 peroxy radicals (RO₂) with nitrous oxide (NO) dominated the formation of RONO₂ at
24 both sites, and the formation of alkyl nitrates contributed negatively to O₃ production,
25 with average reduction rates of -4.1 and -4.7 pptv/pptv at TMS and TW, respectively.

26

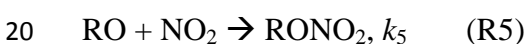
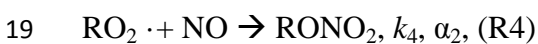
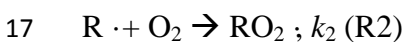
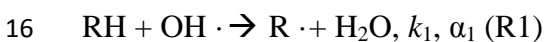
27 **Key word:** Alkyl nitrates; Source apportionment; Secondary formation; Biomass
28 burning

29

1 **1. Introduction**

2 Alkyl nitrates (RONO₂) are important photochemical pollutants in the atmosphere due
3 to their roles in local, regional and global atmospheric chemistry (Jenkin et al., 2000;
4 Seinfeld and Pandis, 2006). Alkyl nitrates are reactive nitrogen compounds (NO_y) and
5 act as a critical reservoir of nitrogen oxides (NO_x = NO + NO₂) during long-range
6 transport due to their relatively low reactivity (Atkinson, 2006).

7 A number of studies conducted in different environments have shown that alkyl
8 nitrates are either emitted from marine sources directly and/or produced indirectly
9 through photochemical reactions (Roberts et al., 1998; Blake et al., 2003; Simpson et
10 al., 2002, 2003, 2006; Reeves et al., 2007; Wang et al., 2013). In the case of biomass
11 burning, secondary alkyl nitrate formation is believed to occur by the photo-oxidation
12 of emitted hydrocarbons with a formation mechanism of RO and NO₂ (Simpson et al.,
13 2002). The photochemical pathways for the secondary formation of alkyl nitrates are
14 expressed as follows (Atkinson et al., 2006; Jenkin et al., 2000; Arey et al., 2001;
15 Sommariva et al., 2008):

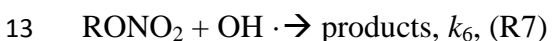


21 where k_1, k_2, k_3, k_4 and k_5 are reaction rate constants. α_1 and α_2 are branching ratios for
22 the corresponding radicals, which increase as the carbon number increases and are
23 dependent on the carbon chain length.

24 Photochemical formation of alkyl nitrates influences the oxidation of NO to NO₂,
25 subsequently leading to O₃ production by NO₂ photolysis. Therefore, alkyl nitrates are
26 often used as indicators of photochemical O₃ production (Simpson et al., 2006).
27 Furthermore, the interactions of alkyl nitrates with their parent hydrocarbons provide
28 useful information about the photochemical processing of air masses. Comparing
29 measured and predicted RONO₂/RH ratios calculated using the laboratory kinetic data
30 as a function of time, Bertman et al. (1995) examined the photochemical evolution of

1 alkyl nitrates at Scotia, Pennsylvania and the Kinterbish Wildlife Area, Alabama.
2 Since then, this approach has been used to investigate the evolution of alkyl nitrates
3 with air mass age in different regions (Simpson et al., 2006; Reeves et al., 2007;
4 Russo et al., 2010; Worton et al., 2010; Wang et al., 2013). Fairly good agreement
5 (>0.5) between measured and modeled ratios suggests that the oxidation of
6 single-parent hydrocarbons represents the evolution of their daughter alkyl nitrates,
7 while poor correlation indicated sources other than photochemical formation of alkyl
8 nitrates.

9 In contrast, the main sinks for ambient alkyl nitrates are photolysis and reactions with
10 hydroxyl radical (OH), making alkyl nitrate lifetimes vary with season, latitude and
11 altitude (days to weeks):



14 where $h\nu$ is sunlight and J_{RONO_2} and k_6 are the photolysis and OH reaction rate
15 constants, respectively. The importance of alkyl nitrate removal by photolysis
16 decreases as the carbon number increases (Clemmitshaw et al., 1997; Talukdar et al.,
17 1997). Dry deposition has recently been recognized as another pathway for the
18 removal of atmospheric alkyl nitrates (Russo et al., 2010; Wu et al., 2011).

19 Despite increased concern over photochemical pollution in Hong Kong and the
20 greater Pearl River Delta (PRD) region, limited studies have focused on the
21 characteristics of alkyl nitrates, which share a common mechanism with
22 photochemical O_3 formation and act as indicators of photochemical processing. For
23 example, based on measurements conducted in 2001-2002, including during ozone
24 episodes, Simpson et al. (2006) analyzed the general characteristics of alkyl nitrates at
25 a coastal site (Tai O) in Hong Kong. C_3 - C_4 alkyl nitrates were the most abundant
26 species, with maximum and minimum levels in winter and summer, respectively. The
27 diurnal variations suggested that photochemical production was the dominant source
28 of alkyl nitrates at Tai O. Furthermore, through approximate calculations, it was
29 concluded that the methoxy radical ($\text{CH}_3\text{O} \cdot$) reaction with NO_2 was a viable
30 alternative pathway for the observed high levels of MeONO_2 during pollution

1 episodes. This mechanism was subsequently verified by Archibald et al. (2007) via
2 box model simulations, whereby $\text{RO} + \text{NO}_2 \rightarrow \text{RONO}_2$ became important for
3 MeONO_2 formation at 10 ppb NO_2 and dominant at 35 ppb NO_2 . However,
4 knowledge related to the chemical evolution and source apportionments of individual
5 alkyl nitrates and their relationship with parent hydrocarbons is still lacking in Hong
6 Kong, especially given that levels of alkyl nitrate precursors have varied since 2002
7 (Ling and Guo 2014). Hence, in this study, intensive field measurements of $\text{C}_1\text{-C}_4$
8 alkyl nitrates were conducted at two sites - a mountain site (Mt. Tai Mo Shan, TMS)
9 and an urban site (Tsuen Wan, TW) at the foot of the same mountain in Hong Kong.
10 The data were analyzed and compared with the previous study conducted at Tai O
11 (Simpson et al., 2006). The aims were to investigate the spatiotemporal variations and,
12 for the first time, source apportionments and photochemical formation pathways and
13 evolution of alkyl nitrates in Hong Kong.

14

15 **2. Methodology**

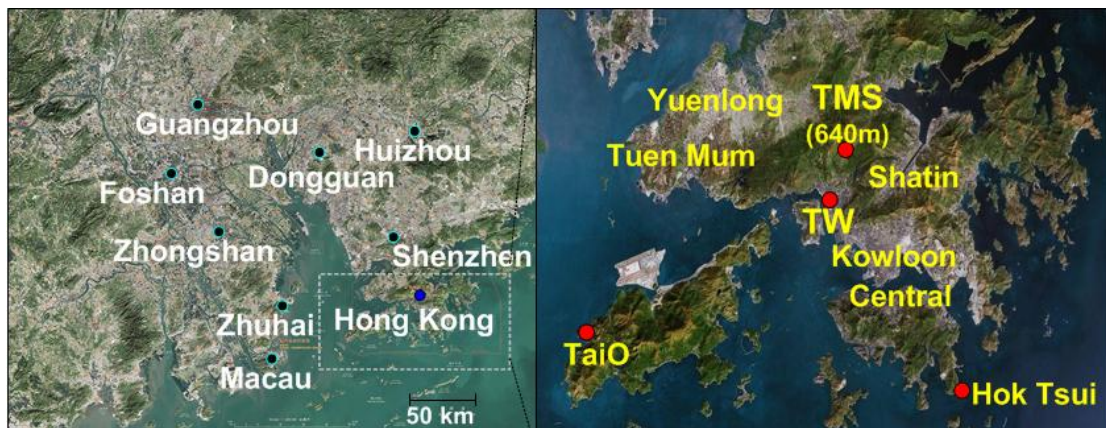
16 **2.1. Sampling sites**

17 In this study, concurrent field measurements were conducted at two sites located at
18 different elevations of the highest mountain, *i.e.*, Mt. Tai Mo Shan (TMS) with an
19 elevation of 957 m a.s.l. in Hong Kong from September 6 to November 29, 2010. A
20 detailed description of the topography of Mt. TMS was provided in an overview paper
21 (Guo et al., 2013a). In brief, Figure 1 presents the two sampling locations and the
22 surroundings. The high-elevation site (TMS) was set on the rooftop of a building on
23 the mountainside (640 m a.s.l.), the highest logistically feasible observation location,
24 beyond which the area comprised the natural landscape with shrubs and grasses to the
25 mountain summit (AFCD, 2008). The measurement site at the foot of the mountain
26 was the monitoring station of the Hong Kong Environmental Protection Department
27 (HKEPD) at Tsuen Wan (TW), a mixed residential, commercial and light industrial
28 area in the New Territories of Hong Kong. The TW monitoring site was located on the
29 rooftop of a building, approximately 15-20 m above ground level. The linear distance
30 between the TMS and TW sites was about 7 km and the difference in elevation

1 between the two sites was 630 m. In general, the solar radiation was comparable at the
2 two sites, while the temperature was higher and the relative humidity and wind speed
3 were lower at the TW site (Guo et al., 2013a). The winds at TMS were generally from
4 the north with speeds ranging from 0.02 to 4 m s⁻¹, and the winds at TW were
5 predominantly from the southeast at speeds of 1-3 m s⁻¹ with easterly winds at night
6 and southerly winds during the day. Due to its unique topography, the air at TMS was
7 often influenced by the mountain-valley breezes and regional transport (Guo et al.,
8 2013a). Based on the average wind speed of 1.9 m/s, air masses transported from
9 upwind locations, on both local (~7 km) and regional scales (~20 km), took
10 approximately 1-3 hours to arrive at the TMS site (Guo et al., 2012, 2013a).

11 The Tai O sampling station was a rural/costal site located on the western coast of
12 Lantau Island in southwestern Hong Kong (elevation, 80 m a.s.l.) (Figure 1). Further
13 to the east are the urban areas, with a straight distance of 32 km, and to the northeast,
14 north and northwest is the polluted PRD region. The Asian monsoon has a significant
15 influence on the seasonal variations of air pollutants at Tai O. In autumn and winter,
16 prevailing northerly winds bring anthropogenic emissions from the PRD region to Tai
17 O, which superimpose with emissions from local urban areas. In summer, clean
18 oceanic air masses dilute the levels of air pollutants because of the influence of
19 dominant southerly winds. A detailed description of the site is provided in Wang et al.
20 (2003).

21



22

23 Figure 1. Tai Mo Shan (TMS) and Tsuen Wan (TW) sampling sites and the
24 surrounding environments in Hong Kong.

2.2. Sampling and analysis of volatile organic compounds (VOCs)

Whole air samples were collected on 10 O₃ episode days and 10 non-O₃ episode days using evacuated 2-L stainless steel canisters. Each of the collected canister samples was integrated over a 60-min sampling duration. A total of 384 samples were collected at the two sites. The O₃ episode days were selected as the days with the highest daytime hourly O₃ level at a regional scale (higher than 100 ppbv), which were based on weather forecasts and meteorological data analysis, and confirmed by the observed O₃ mixing ratios. During non-O₃ episode days, one-hour integrated samples were collected at 2-h intervals from 0700 to 1900 local time (LT) (7 samples per day). On O₃ episode days, one-hour integrated samples were collected from 0900 to 1600 LT at 1-h intervals with additional integrated samples collected at 1800, 2100, 0000, 0300 and 0700 LT (a total of 13 samples per day). After the campaign, the canister samples were sent to the University of California, Irvine (UCI) for chemical analysis. Other studies have provided detailed descriptions of the analytical system and the quality control, detection limits and analysis precision of the VOC samples (Simpson et al., 2006, 2010). In brief, the precision and detection limit of the alkyl nitrate measurements is 5% and 0.02 pptv, respectively. The calibration scale for the alkyl nitrate measurements changed in 2008, increasing by factors of 2.13, 1.81, 1.24 and 1.17 for the C₁, C₂, C₃ and C₄ alkyl nitrates, respectively (Simpson et al., 2011). In other words, the alkyl nitrates reported at Tai O by Simpson et al. (2006) were lower than the data reported here, and the Tai O data have been adjusted to the new calibration scale to allow direct comparison with this work. The Tai O sampling campaign was conducted from 24 August 2001 to 31 December 2002. Different from the air samples collected at TMS and TW, each whole-air sample at Tai O was collected for only 1-min, and was then analyzed at UCI. Intensive sampling from 0700-1900 LT was conducted every 2-h during the selected pollution episodes (17-19 October 2001, 29-30 August, 5-6 September, 9-11 and 25 October, 6-8 and 12 November 2002). Apart from the intensive sampling days, samples were taken either daily or every few days, typically in the midafternoon (Simpson et al., 2006).

2.3. Continuous measurements of O₃, CO and NO-NO₂-NO_x

1 At TMS, online measurements of O₃, CO and NO-NO₂-NO_x were made using
2 commercial analyzers. O₃ was measured using a commercial UV photometric
3 instrument (Advanced Pollution Instrumentation (API), model 400E) that has a
4 detection limit of 0.6 ppbv. CO was measured with a gas filter correlation,
5 nondispersive infrared analyzer (API, Model 300E) with a heated catalytic scrubber
6 (as purchased) to convert CO to carbon dioxide (CO₂) for baseline determination. The
7 detection limit was 30 ppbv for a 2-min average. The 2s precision was about 1% for a
8 level of 500 ppbv (2- min average) and the overall uncertainty was estimated to be
9 10%. NO, NO₂ and NO_x were detected with a chemiluminescence NO-NO₂-NO_x
10 analyzer (API, Model 200E) that had a detection limit of 0.5 ppbv. The O₃ analyzer
11 was calibrated by a transfer standard (Thermo Environmental Instruments (TEI)
12 49PS), while the other analyzers were calibrated daily by injecting scrubbed ambient
13 air (TEI, Model 111) and a span gas mixture weekly with a NIST (National Institute
14 of Standards and Technology) traceable standard (Scott-Marrin, Inc.), containing
15 156.5 ppmv CO (± 2 %), 15.64 ppmv SO₂ (± 2 %), and 15.55 ppmv NO (± 2 %), which
16 was diluted using a dynamic calibrator (EnviroNics, Inc., Model 6100). For the O₃,
17 CO, NO and NO_x analyzers, a data logger (Environmental Systems Corporation
18 Model 8816) was used to control the calibrations and to collect data, which were
19 averaged to 1-min values.

20 In addition to the above chemical measurements, several meteorological parameters,
21 including wind speed and direction, temperature, relative humidity and solar radiation,
22 were measured by the integrated sensor suite (Vantage Pro TM & Vantage Pro 2 Plus
23 TM Weather Stations, Davis Instruments).

24 At TW, hourly O₃, CO, NO-NO₂-NO_x and meteorological data were obtained from
25 the HKEPD (<http://epic.epd.gov.hk/ca/uid/airdata>). The hourly data were derived by
26 averaging 1-min data subsequently over the same time interval as the TMS data.
27 Detailed information about the measurements, quality assurance and control protocols
28 can be found in the HKEPD report (HKEPD, 2012). In addition, Table S1 in the
29 supplementary information shows descriptive statistics of main non-methane
30 hydrocarbons (NMHCs) and trace gases at both sites.

1 **2.4. Positive Matrix Factorization (PMF) model**

2 In this study, the US EPA PMF 3.0 (<http://www.epa/heads/products/pmf/pmf.html>)
3 was used for the source apportionments of the observed alkyl nitrates at TW. Our
4 previous studies provided detailed information about the PMF model (Ling et al.,
5 2011; Ling and Guo, 2014). In terms of the PMF input, the uncertainty for each
6 species was determined as the sum of 10% of the VOC concentration and two times
7 the method detection limit (MDL) of the species (Paatero, 2000). Tracers for different
8 sources were selected for the model input. For example, CO, ethane and ethyne were
9 the tracers of combustion processes, and CH₃Cl was specifically used for biomass
10 burning. DMS was a typical tracer for marine emissions, while O_x (*i.e.*, O₃ + NO₂)
11 was used as the tracer of secondary formation through photochemical reactions
12 including the formation of alkyl nitrates because O₃ shares a common photochemical
13 source with alkyl nitrates (Simpson et al., 2006). In addition to the aforementioned
14 species, alkyl nitrate precursors, including methane, propane and *n/i*-butanes, were
15 input into the model. In total, sixteen compounds were used for the model input.
16 Different checks and sensitivity tests were conducted to examine the model
17 performance. Firstly, many different starting seeds were tested and no multiple
18 solutions were found. Secondly, good correlation between the observed and predicted
19 VOC concentrations at TMS and TW ($R^2 = 0.99$ and 0.98 , respectively) was found
20 after the PMF implementation. Thirdly, the scale residuals, which are the uncertainty
21 over the different runs for the input species, ranged between -3 and 3 for the PMF
22 solution. The Q values were stable and the Q values in the robust mode were
23 approximately equal to the degrees of freedom (EPA, 2008; Friend et al., 2010). All
24 the factors were mapped to a base factor in all the 100 runs in the bootstrapped
25 simulation for the three-factor solution, suggesting the solution was stable. Lastly, the
26 G-space plot extracted from the F-peak model results did not present oblique edges,
27 reflecting that there was little rotation for the selected solution. Overall, the above
28 features demonstrated that PMF provided reasonable results for the source
29 apportionment of alkyl nitrates (Ling et al., 2011; Ling and Guo, 2014).

30 **2.5. Photochemical box model incorporating master chemical mechanism**

1 (PBM-MCM)

2 A photochemical box model coupled with Master Chemical Mechanism (PBM-MCM)
3 was used to simulate the in-situ formation of alkyl nitrates at TMS and TW. The
4 PBM-MCM was developed by assuming that it was a well-mixed box without the
5 treatment of vertical or horizontal dispersion, and the air pollutants in the model were
6 homogeneous. For the mechanism coupled in the model, the MCM (version 3.2) used
7 in this study is a state-of-the-art chemical mechanism, which describes the
8 degradation of 143 primary VOCs including methane and contains around 16,500
9 reactions involving 5900 chemical species (Jenkin et al., 1997, 2003; Saunders et al.,
10 2003). The measured data, including O₃, CO, NO_x, SO₂, 54 VOCs and methane,
11 together with the actual meteorological conditions of temperature, relative humidity
12 and boundary layer in the region, were used to constrain the model. The photolysis
13 rates of different species in the model were parameterized as suggested by the
14 previous study (Pinho et al., 2009) using the photon flux determined from the
15 Tropospheric Ultraviolet and Visible Radiation (v5) model based on the actual
16 conditions, such as meteorological conditions, location and time period of the field
17 campaign in Hong Kong (Lam et al., 2013). The model output simulated in-situ
18 formation of alkyl nitrates and other secondary products as well as the full set of
19 precursors, radicals and intermediates. To provide robust results from the model
20 simulation, several measures were adopted for the model development. The detailed
21 information for the model frameworks, the model development and the evaluation for
22 the model performance has been reported in our previous studies (Lam et al., 2013;
23 Ling et al., 2014).

24

25 3. Results and discussion

26 3.1 Descriptive statistics of alkyl nitrates and their parent hydrocarbons

27 Table 1 presents the descriptive statistics of alkyl nitrates and their parent
28 hydrocarbons at TMS and TW. Figure 2 compares the levels of alkyl nitrates
29 measured at TMS and TW with those measured in different environments in previous
30 studies. In general, 2-PrONO₂ and 2-BuONO₂ were the most abundant alkyl nitrates

1 at the two sites, consistent with the results observed in different environments (Blake
2 et al., 2003; Simpson et al., 2006; Russo et al., 2010; Wang et al., 2013). The
3 relatively higher levels of 2-PrONO₂ and 2-BuONO₂ were due to the balance between
4 increased branching ratios for photochemical alkyl nitrate formation and the
5 decreased lifetime of both parent alkanes and alkyl nitrates with increasing carbon
6 number (Arey et al., 2001; Simpson et al., 2006; Russo et al., 2010). In comparison,
7 the levels of MeONO₂, EtONO₂ and 2-PrONO₂ were slightly higher at TW than at
8 TMS ($p < 0.05$), with average values of 12.6 ± 0.5 (mean \pm 95% confidence interval),
9 13.3 ± 0.6 and 26.3 ± 1.2 pptv, respectively, at TW. The average mixing ratios of
10 1-PrONO₂ and 2-BuONO₂ were comparable at the two sites ($p > 0.05$). The results
11 were contradictory to the fact that the mixing ratios of their parent hydrocarbons at
12 TMS were much lower than at TW, highlighting the complexity of sources of alkyl
13 nitrates at both sites.

14 In comparison with other studies, the average mixing ratios of alkyl nitrates at TMS
15 were much higher than those measured in forested areas in coastal New England
16 (Russo et al., 2010) and in tropospheric air influenced by Asian outflow during the
17 airborne TRACE-P mission (Simpson et al., 2003), where the levels of parent
18 hydrocarbons were also lower. (Note that all of the UCI data shown in Figure 2 were
19 adjusted to UCI's post-2008 alkyl nitrates' calibration scale to enable direct
20 comparison (Simpson et al., 2011)). However, the mean mixing ratios of C₁-C₃ alkyl
21 nitrates were slightly lower and the 2-BuONO₂ mixing ratio was higher at TMS than
22 at Tai O (Table 2), Hok Tsui and in Karachi, Pakistan (Barletta et al., 2002; the
23 Karachi data have also been adjusted to the new UCI alkyl nitrates' calibration scale).
24 The differences among TMS, Tai O and Hok Tsui might result not only from the
25 levels of their parent hydrocarbons, but also from the influence of air masses with
26 different photochemical ages and sources (Wang et al., 2003). Furthermore, as
27 mentioned in Section 2.2, the sampling method and sampling period at TMS were
28 different from those at Tai O and Hok Tsui, where the sampling duration was only
29 1-min and the sampling time varied on different sampling days. In particular, many
30 whole air samples were collected during O₃ episodes at Tai O. These could also

1 induce differences in observed levels among the three sites. At the urban TW site, the
 2 mean mixing ratios of alkyl nitrates were lower than those measured in urban areas in
 3 Europe (Worton et al., 2010) and China (Wang et al., 2013). Compared to the average
 4 values of alkyl nitrates at Tai O, the levels of EtONO₂, 1-PrONO₂ and 2-BuONO₂
 5 were slightly higher and the MeONO₂ and 2-PrONO₂ mixing ratio was lower at TW.

6

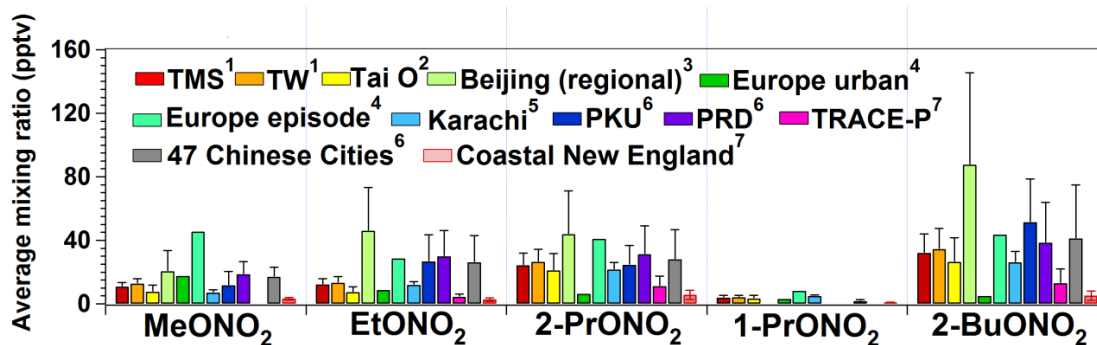
7 Table 1 Descriptive statistics of alkyl nitrates and parent hydrocarbons (pptv) in whole
 8 air samples collected at TMS and TW during the sampling period.

| Species | TMS | | | TW | | |
|----------------------|----------|------|------|----------|------|-------|
| | Mean* | Min. | Max. | Mean | Min. | Max. |
| MeONO ₂ | 10.9±0.4 | 6.2 | 21.4 | 12.6±0.5 | 7.2 | 26.6 |
| EtONO ₂ | 12.1±0.5 | 3.2 | 25.6 | 13.3±0.6 | 4.0 | 35.0 |
| 2-PrONO ₂ | 24.1±1.1 | 4.0 | 51.2 | 26.3±1.2 | 6.0 | 49.2 |
| 1-PrONO ₂ | 3.8±0.2 | 0.4 | 10.6 | 4.0±0.2 | 0.7 | 8.1 |
| 2-BuONO ₂ | 32.0±1.7 | 3.1 | 80.1 | 34.2±1.9 | 5.1 | 92.8 |
| Methane (ppmv) | 2.0±0.1 | 1.8 | 2.2 | 2.0±0.1 | 1.8 | 2.5 |
| Ethane | 1908±78 | 396 | 3588 | 2224±90 | 717 | 4315 |
| Propane | 1101±75 | 106 | 4455 | 3551±415 | 1443 | 33800 |
| <i>n</i> -Butane | 830±91 | 97 | 6252 | 4486±482 | 1372 | 34700 |

9 * Average ± 95% confidence interval

10

11



12

13 Figure 2. Comparison of alkyl nitrate mixing ratios in different locations. Data
 14 collected by UCI before 2008 (PRD and TRACE-P) were adjusted to UCI's new
 15 calibration scale to permit direct comparison (see text for details about the new
 16 calibration.

17 ¹ This study, September-November, 2010. ² Rural site, August 2001-December 2002 (Simpson et
 18 al., 2006). ³ Urban site, 2009-2011 (Wang et al., 2013). ⁴ Urban sites, April-May 2004 (Worton et
 19 a., 2010). ⁵ Urban sites, April-May 2004 (Worton et al., 2010). ⁶ Coastal site, December
 20 1998-January 1999 (Barletta et al., 2002). ⁷ Urban site, August-September 2011 and December
 21 2011-January 2012 (Wang et al., 2013). ⁸ Regional background sites, September 2009 (Wang et al.,
 22 2013). ⁹ Aircraft measurement, February-April 2001 (Simpson et al., 2003). ¹⁰ Urban sites, July

1 2009 (Wang et al., 2013). ¹¹ Coastal site, January-February and June-August 2002, July-August
2 2004 (Russo et al., 2010). ¹² Regional background site, March 2001-April 2002 (unpublished
3 data).

4

5

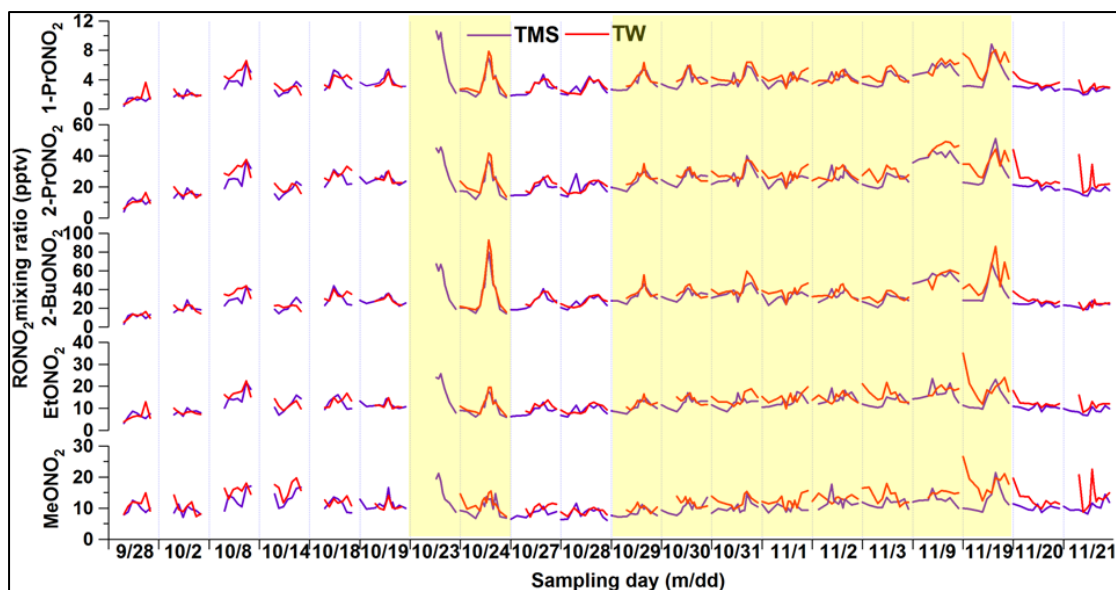
6 Table 2 Descriptive statistics of alkyl nitrate (pptv) and parent hydrocarbons (ppbv) in
7 whole air samples collected at Tai O between 24 August 2001 and 31 December 2002
8 (from Simpson et al., 2006).

| Compound | Minimum | Maximum | Median | Mean |
|-------------------------|---------|---------|--------|------|
| MeONO ₂ | 5.5 | 52.2 | 13.4 | 15.9 |
| EtONO ₂ | 2.7 | 34.3 | 12.1 | 13.1 |
| 1-PrONO ₂ | 0.2 | 14.5 | 3.5 | 3.9 |
| 2-PrONO ₂ | 2.4 | 65.9 | 24.5 | 32.6 |
| 2-BuONO ₂ | 0.8 | 89.8 | 27.4 | 30.7 |
| Methane (ppmv) | 1.75 | 3.70 | 1.96 | 2.05 |
| Ethane (ppbv) | 0.38 | 5.05 | 2.14 | 2.12 |
| Propane (ppbv) | 0.006 | 13.0 | 1.54 | 2.05 |
| <i>n</i> -Butane (ppbv) | 0.006 | 12.8 | 0.95 | 1.64 |

9

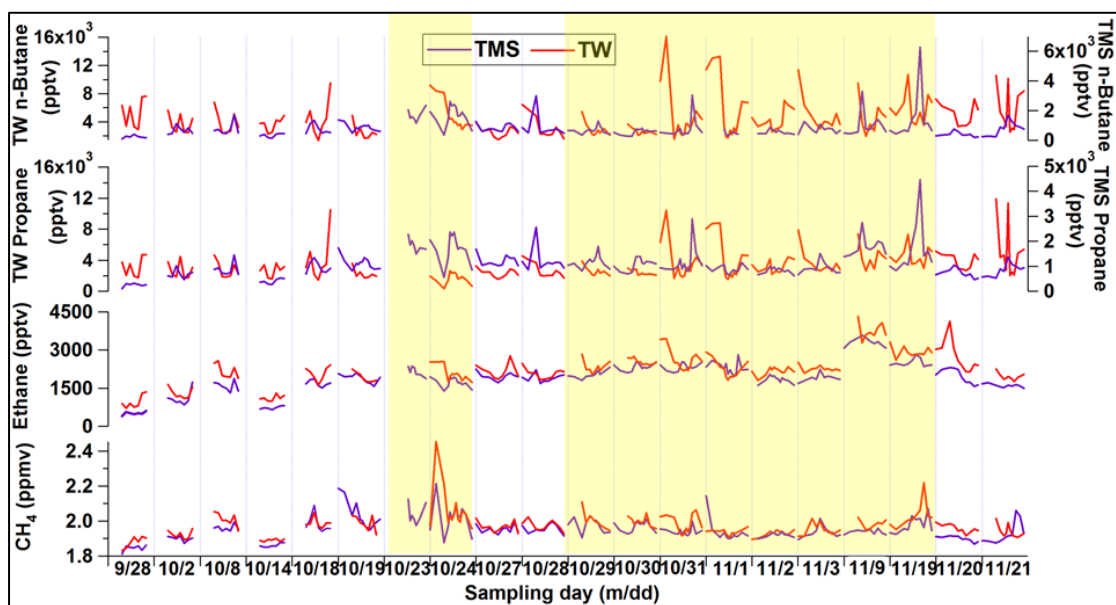
10 Table S2 and Figure S1 in the supplementary information summarize the synoptic
11 weather conditions and the corresponding variations of O₃ and alkyl nitrates on O₃
12 episode and non-O₃ episode days at both sites. In general, weather conditions
13 including temperatures, winds and solar radiation significantly influenced the levels
14 of air pollutants (Table S2). High mixing ratios of O₃ and alkyl nitrates were usually
15 associated with weather conditions with high-pressure system and/or stable weather
16 conditions, such as high temperatures, intense solar radiation and low wind speeds.
17 Figure 3 shows the time series of C₁-C₄ alkyl nitrates on O₃ episode and non-O₃
18 episode days at both sites, while Figure 4 presents the temporal variations of their
19 parent hydrocarbons accordingly. Although the ranges of alkyl nitrate mixing ratios
20 were similar and peak values were observed in the afternoon, the day-to-day
21 variations of individual alkyl nitrates differed during the sampling period at both sites.
22 The peak values were comparable and the diurnal patterns well tracked each other for
23 C₃-C₄ alkyl nitrates at TMS and TW, especially on the days (24 October to 3
24 November, 9 and 19 November) with relatively higher O₃ mixing ratios ($p < 0.05$).
25 The average daytime O₃ mixing ratios (0700-1800) on the high O₃ days were 77 ± 3

1 and 38 ± 3 ppbv at TMS and TW, respectively, compared to 58 ± 3 and 23 ± 3 ppbv,
2 respectively, on the non-O₃ episode days. Typically, the average daytime levels of
3 2-PrONO₂, 1-PrONO₂ and 2-BuONO₂ on high-level O₃ days at TMS were 27 ± 1
4 (TW: 28 ± 1), 4.5 ± 0.3 (4.4 ± 0.2) and 37 ± 2 (39 ± 3) pptv, respectively, higher than
5 those on non-O₃ episode days ($p < 0.05$), implying that secondary formation of alkyl
6 nitrates might be more prominent on O₃ episode days. Coincident with the high C₃-C₄
7 alkyl nitrates during high O₃ days, their parent hydrocarbons, *i.e.*, propane (0.56-4.46
8 and 1.55-10.4 ppbv for TMS and TW, respectively) and *n*-butane (0.28-6.25 and
9 1.47-16.1 ppbv, respectively) also showed elevated mixing ratios (Figure 4), further
10 suggesting an important source of C₃-C₄ alkyl nitrates which was photo-oxidation of
11 parent hydrocarbons. For C₁-C₂ alkyl nitrates, the patterns of peaks and troughs of
12 MeONO₂ and EtONO₂ were different at the two sites, especially on high-level O₃
13 days. The peaks of MeONO₂ and EtONO₂ were usually observed between 11 a.m. and
14 4 p.m. at TMS, except for 14 and 28 October, 1-2, 9, 20-21 November. The peaks of
15 C₁-C₂ alkyl nitrates corresponded to the high levels of methane and ethane observed
16 at 11 a.m. to 5 p.m., likely indicative of photo-oxidation of methane and ethane, apart
17 from potential influence of air masses in upwind areas due to regional transport (Guo
18 et al., 2009; Jiang et al., 2010) and/or mesoscale circulations (Gao et al., 2005; Wang
19 et al., 2006). At TW, however, besides the peak concentrations observed in the
20 afternoon, high levels of MeONO₂ and EtONO₂ were observed from midnight to early
21 morning on 13 out of the 19 sampling days (*i.e.*, 2, 8, 14, 24, 28, 30-31 October, 1-3,
22 19-21 November), when the prevailing winds switched to the southeast direction,
23 implying that the high levels of MeONO₂ and EtONO₂ might be related to marine
24 emissions and aged continental plumes which were re-circulated from the South
25 China Sea to the coastal urban site at night. Indeed, this speculation was supported by
26 the source apportionment results at TW, which confirmed that the high MeONO₂ and
27 EtONO₂ levels from midnight to early morning on the above sampling days were
28 related to oceanic emissions (see Section 3.2.2 for details).



1
2
3
4
5

Figure 3. Time series of MeONO₂, EtONO₂, 1-PrONO₂, 2-PrONO₂ and 2-BuONO₂ measured at TMS (purple) and TW (red) in 2010. The yellow shading highlights the O₃ episode days.



6
7
8
9

Figure 4. Time series of the parent hydrocarbons of alkyl nitrates at TMS and TW. The yellow shading highlights the O₃ episode days.

10 Overall, though the levels of the parent hydrocarbons were lower at TMS, similar
11 values of alkyl nitrates were observed at both sites regardless of different elevations
12 of the sites, suggesting the contributions of different sources and/or the influence of
13 different air masses. Hence, the source apportionments of alkyl nitrates, contributions
14 of reaction pathways for the secondary formation of alkyl nitrates, and the

1 relationship between O₃ and alkyl nitrates were in-depth studied in the following
2 sections.

3 **3.2. Sources of alkyl nitrates**

4 **3.2.1. Photochemical evolution of alkyl nitrates**

5 As photochemical oxidation of parent hydrocarbons is an important source of alkyl
6 nitrates, it is helpful to study the photochemical evolution of alkyl nitrates. To do so,
7 the relationships of alkyl nitrates with their parent hydrocarbons at the two sites were
8 further examined using a simplified sequential reaction model developed by Bertman
9 et al. (1995) (Equation 1), based on the assumptions that: (i) the hydrogen abstraction
10 reaction from the parent hydrocarbon was the rate-limiting step for photochemical
11 production of alkyl nitrates, and (ii) the reaction environment was NO_x-rich, making
12 the reaction with NO being the dominant pathway for the destruction of RO₂ radicals
13 (Russo et al., 2010). In this study, the average mixing ratios of NO_x at TMS and TW
14 were 10.7 ± 0.3 and 56.3 ± 1.6 ppbv, respectively, indicating that the environment was
15 NO_x-rich (> 0.1 ppbv, Roberts et al., 1998). Hence, reaction with NO was the main
16 pathway for the destruction of RO₂ radicals at the two sites. In addition, the results of
17 PBM-MCM model simulation confirmed that the hydrogen abstraction reaction from
18 the parent hydrocarbon, namely the reaction of hydrocarbon with OH radical, was
19 indeed the rate-limiting step for photochemical production of alkyl nitrates at both
20 sites (Lyu et al., 2015).

$$21 \quad \frac{RONO_2}{RH} = \frac{\beta k_A}{k_B - k_A} (1 - e^{(k_A - k_B)t}) + \frac{[RONO_2]_0}{[RH]_0} e^{(k_A - k_B)t} \quad (\text{Eq. 1})$$

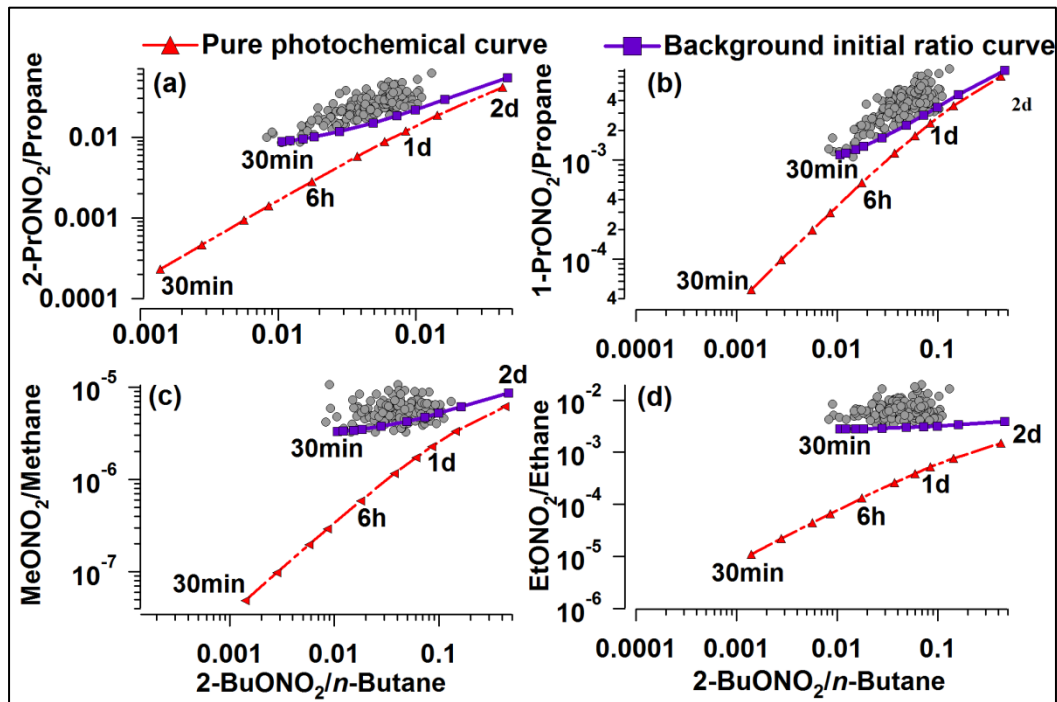
22 where $\beta = \alpha_1 \alpha_2$, k_A is the production rate for the formation of alkyl nitrates through the
23 oxidation of hydrocarbons, RH ($k_A = k_1[\text{OH}]$), while k_B is the destruction rate for alkyl
24 nitrates through photolysis and the reaction with OH ($k_B = k_5[\text{OH}] + J_{\text{RONO}_2}$).
25 $[RONO_2]_0$ and $[RH]_0$ are the initial concentrations of alkyl nitrates and the parent
26 hydrocarbons before photochemical processing, respectively. $[\text{OH}]$ is the diurnal
27 average concentration of the OH radical. The relationships of alkyl nitrates with their
28 parent hydrocarbons derived from the preceding equation are comparatively
29 independent of the variations of OH and photolysis rates of alkyl nitrates (Roberts et

1 al., 1998; Wang et al., 2013). If the initial concentrations of alkyl nitrates and RH are
2 zero, Equation 1 can be expressed as follows (Equation 2):

$$3 \frac{RONO_2}{RH} = \frac{\beta k_A}{k_B - k_A} (1 - e^{(k_A - k_B)t}) \quad (2)$$

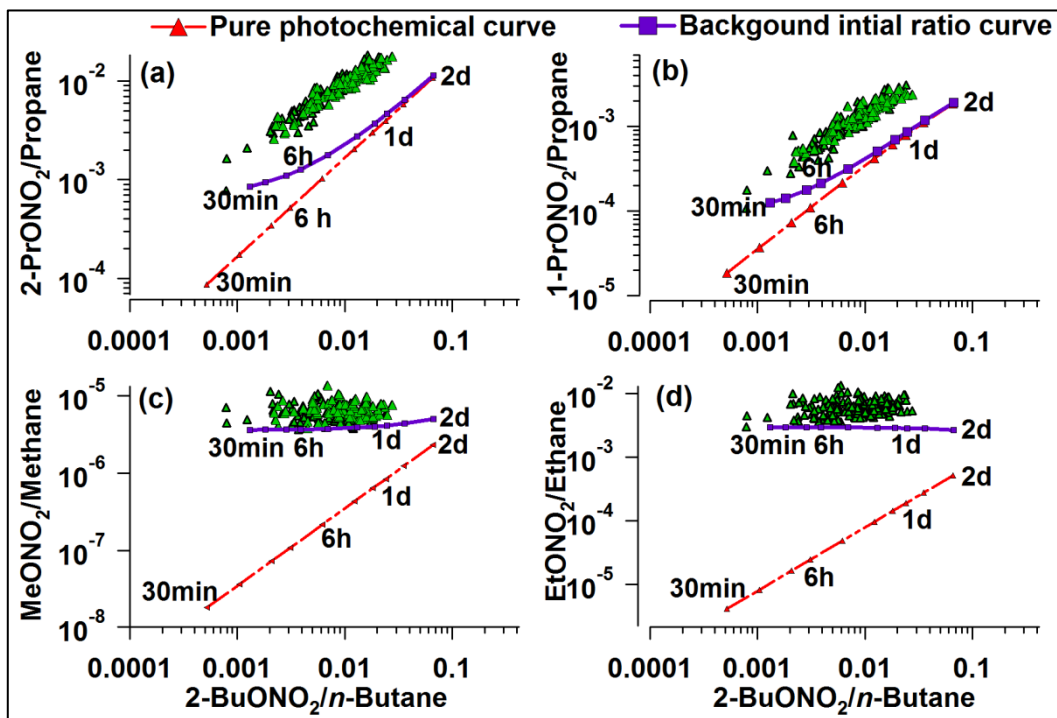
4 The relationships between alkyl nitrates and RH are obtained by plotting the measured
5 ratios of $RONO_2/RH$ to a specific ratio, 2-BuONO₂/*n*-butane. The
6 2-BuONO₂/*n*-butane ratio has been widely used in the analysis of alkyl nitrates because
7 *n*-butane is typically one of the most abundant hydrocarbons and 2-BuONO₂ is the
8 most dominant alkyl nitrate (Roberts et al., 1998; Wang et al., 2013; Worton et al.,
9 2010). Although some studies have investigated the relationships between alkyl
10 nitrates and their parent hydrocarbons using zero initial values of alkyl nitrates, more
11 recent studies have used non-zero initial values of alkyl nitrates to evaluate the
12 influence of background levels on the photochemical evolution of alkyl nitrates
13 (Reeves et al., 2007; Russo et al., 2010; Wang et al., 2013). Therefore, in addition to
14 zero initial ratios, non-zero initial ratios of $RONO_2/RH$, equal to the lowest values
15 from 0000 to 0700 measured at TMS and TW, respectively, as suggested by Wang et
16 al. (2013), were used to investigate the relationships between alkyl nitrates and their
17 parent hydrocarbons in this study. The diurnal average OH mixing ratios [OH] were
18 simulated using the PBM-MCM (Lyu et al., 2016). By providing the values of
19 photochemical processing time (*t*), the predicted ratios of $RONO_2/RH$ were calculated
20 since other parameters, *i.e.*, k_A , k_B , α_1 , α_2 and J_{RONO_2} could be obtained from literatures
21 (Clemmshaw et al., 1997; Simpson et al., 2003; Worton et al., 2010; Wang et al., 2013).
22 In this study, the given photochemical processing time ranged from 30 min to 2 days.
23 The curves generated with zero initial values were the pure photochemical (PP)
24 curves for the evolution of alkyl nitrates, and the curves with non-zero values, defined
25 as background initial ratio (BIR) curves, were generated by assuming that both
26 photochemical formation and background levels contributed to the distribution of
27 alkyl nitrates (Russo et al., 2010; Wang et al., 2013). Consistent with previous studies
28 (Russo et al., 2010; Wang et al., 2013), the shapes of the BIR curves were different
29 from those of PP curves. The BIR curves of C₁-C₃ alkyl nitrates at both sites laid

1 above their PP curves at shorter processing time ($t < 1$ d) and converged towards the
 2 PP curves at longer processing times ($t = 1.5-2$ d) (Figure 5), resulting from the
 3 decreased influence of the parameter $\frac{[RONO_2]_0}{[RH]_0} e^{(k_A - k_B)t}$ on the difference between
 4 the two curves as the photochemical age increased (Wang et al., 2013). This feature
 5 was more pronounced for C₃-C₄ alkyl nitrates at TW (Figure 6) because of the lower
 6 values of $[RONO_2]_0/[RH]_0$ resulting from the high mixing ratios of propane and
 7 *n*-butane (Ling and Guo, 2014). Figure 5 presents the relationships of C₁-C₃
 8 RONO₂/RH to 2-BuONO₂/*n*-butane at TMS. The red dashed curves are pure
 9 photochemical curves, while the blue solid curves are BIR curves with the lowest
 10 ratios of RONO₂/RH from 0000 to 0700 LT as the background initial ratio. Similarly,
 11 Figure 6 shows the relationships of C₁-C₃ RONO₂/RH to 2-BuONO₂/*n*-butane at TW.



12
 13 Figure 5. Relationships of C₁-C₃ RONO₂/RH with 2-BuONO₂/*n*-butane at TMS. The
 14 red dashed curves were obtained based on zero initial concentrations of RH and alkyl
 15 nitrates (pure photochemical curves, PP), while the blue solid curves were obtained
 16 based on non-zero initial levels (background initial ratio curves, BIR), with the lowest
 17 ratios of RONO₂/RH from 0000 to 0700 LT.

18



1

2 Figure 6. Relationships of C₁-C₃ RONO₂/RH with 2-BuONO₂/*n*-butane at TW. The
 3 red dashed curves were obtained based on zero initial concentrations of RH and alkyl
 4 nitrates (pure photochemical curves, PP), while the blue solid curves were obtained
 5 based on non-zero initial levels (background initial ratio curves, BIR), with the lowest
 6 ratios of RONO₂/RH from 0000 to 0700 LT.

7

8 At TMS, the measured ratios of MeONO₂/methane and EtONO₂/ethane to
 9 2-BuONO₂/*n*-butane were much higher than the ratios in the PP curves (Figure 5c &
 10 d), with the observed ratios larger than their theoretical ratios by factors of 5-25. As
 11 expected, the observed trends approached the PP curves at a longer processing time,
 12 suggesting that the measured ratios of C₁-C₂ RONO₂/RH to 2-BuONO₂/*n*-butane were
 13 influenced by aged air masses due to long atmospheric lifetimes and slow
 14 photochemical degradation rates of methane and ethane (Worton et al., 2010; Russo et
 15 al., 2010). However, the difference between the measured ratios and the predicted
 16 ratios of C₁-C₂ RONO₂/RH to 2-BuONO₂/*n*-butane in BIR curves was comparatively
 17 smaller, further confirming that there were other sources contributing to ambient
 18 C₁-C₂ alkyl nitrates besides photochemical formation, including the background levels
 19 of C₁-C₂ alkyl nitrates and their parent hydrocarbons (direct measurements of RH in
 20 Table 1) (Wang et al., 2013). Indeed, our previous field measurements at Hok Tsui, a

1 PRD regional background site, presented average MeONO₂ and EtONO₂ mixing
2 ratios of 10.4 ± 0.7 and 9.6 ± 0.7 pptv (non-published data, 2001-2002), respectively,
3 which were non-negligible values.

4 With regard to C₃ alkyl nitrates, the measured ratios of 1- and 2-PrONO₂/propane to
5 2-BuONO₂/*n*-butane were closer to the ratios of the BIR curve than those of the PP
6 curve at TMS, further revealing the influence of background C₃ alkyl nitrates and
7 their parent hydrocarbons. However, the evolution of the measured ratios of C₃
8 RONO₂/RH to 2-BuONO₂/*n*-butane agreed well with the predicted ratios of BIR and PP
9 curves at TMS, indicating that secondary formation from propane oxidation
10 contributed significantly to the ambient C₃ alkyl nitrates, including the background C₃
11 alkyl nitrates. Consistent with previous studies, the slopes of the observed ratios of C₃
12 RONO₂/RH to 2-BuONO₂/*n*-butane were different from those in the PP and BIR
13 curves (Russo et al., 2010; Wang et al., 2013). For example, the slopes of the observed
14 ratios of 1- and 2-PrONO₂/propane to 2-BuONO₂/*n*-butane were 0.04 ± 0.01 and 0.26
15 ± 0.02 , respectively, while the slopes for the BIR curves were 0.02 ± 0.01 (PP curve:
16 0.02 ± 0.01) and 0.12 ± 0.01 (0.10 ± 0.01), respectively. This was reasonable due to
17 the difference in the number of samples and distribution of data between the observed
18 ratios and the ratios of PP and BIR curves, particularly when the observed ratios were
19 higher than the theoretical ones due to significant influence of the background levels
20 of alkyl nitrates and RH (Russo et al., 2010; Wang et al., 2013). Therefore, to further
21 investigate the influence of secondary formation and background mixing ratios on C₃
22 alkyl nitrates at TMS, the ratio of 1-/2-PrONO₂ was examined. Previous studies
23 reported that the theoretical ratio of 1-/2-PrONO₂ was the ratio between the yield for
24 1-PrONO₂ and 2-PrONO₂ formation, which was equal to the ratio of
25 $\beta_{1\text{-PrONO}_2}/\beta_{2\text{-PrONO}_2}$ (0.21) (Simpson et al., 2003; Wang et al., 2013). If photochemical
26 production was the dominant source of 1-PrONO₂ and 2-PrONO₂, the observed ratios
27 should be close to the theoretical ones. Indeed, the slope of 1-PrONO₂ and 2-PrONO₂
28 at TMS was 0.19 ($R^2 = 0.86$, $p < 0.05$), close to the theoretical ratio (0.21), confirming
29 that photochemical production from propane, including in-situ photochemical
30 production and transport of photochemically-formed C₃ alkyl nitrates in urban areas

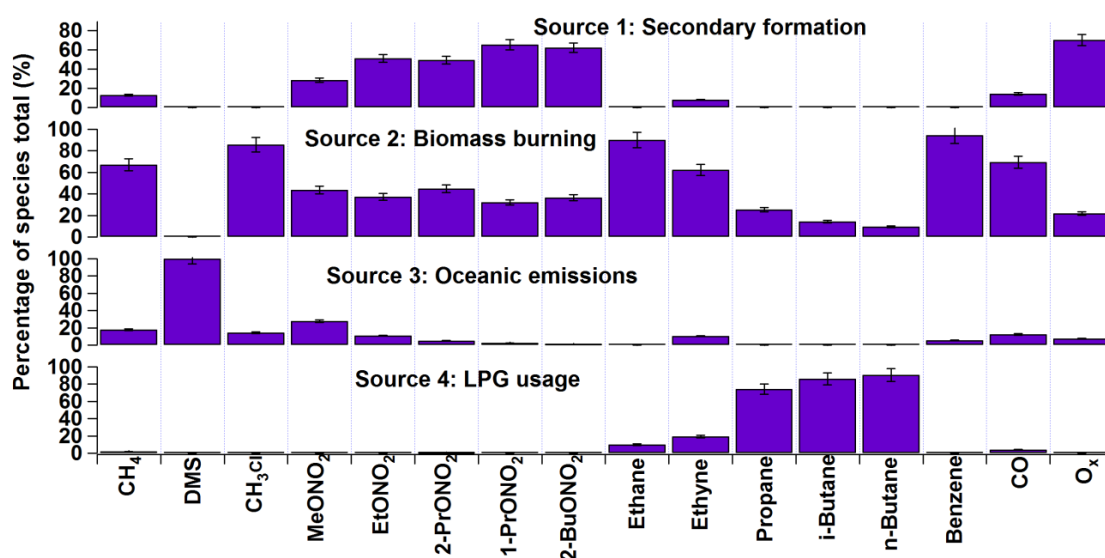
1 and/or during transit from urban areas to TMS, was the dominant source of ambient
2 C₃ alkyl nitrates.

3 At TW, the comparison between the observed ratios of C₁-C₂ RONO₂/RH to
4 2-BuONO₂/*n*-butane and the ratios from the PP and BIR curves was consistent with
5 that at TMS. However, in terms of C₃ alkyl nitrates, although the evolution of the
6 measured ratios of C₃ RONO₂/RH to 2-BuONO₂/*n*-butane followed the trends of the
7 ratios in the PP and BIR curves, the measured ratios of C₃ RONO₂/RH to
8 2-BuONO₂/*n*-butane at TW were further away from the PP/BIR curves, about 2-3
9 times the ratios in the PP and BIR curves, implying additional sources of C₃ alkyl
10 nitrates (Wang et al., 2013) (details in Section 3.2.2). High emissions of propane
11 provided sufficient precursors of C₃ alkyl nitrates, and the lifetimes of 1-PrONO₂ and
12 2-PrONO₂ were long enough to sustain relatively high levels at TW. To further
13 investigate the influence of additional sources on the distributions of C₃ alkyl nitrates
14 at TW, equation 1 was used to fit the measured ratios of 1- and 2-PrONO₂/propane to
15 calculate the yield of C₃ alkyl nitrates (β). The average yields of 1- and 2-PrONO₂
16 were 0.032 ± 0.004 and 0.22 ± 0.02 , respectively, higher than the laboratory kinetic
17 values by factors of 4–9 (Kwok and Atkinson, 1995), confirming the existence of
18 additional emissions of C₃ alkyl nitrates at TW, including locally-emitted C₃ alkyl
19 nitrates and/or secondary formation other than the production pathway from propane
20 to proxyl radical and PrONO₂ (Reeves et al., 2007; Worton et al., 2010). Indeed, the
21 slope of 1-PrONO₂ to 2-PrONO₂ at TW was 0.15 ($R^2 = 0.80$, $p < 0.05$), lower than the
22 theoretical ratio of 0.21, further demonstrating the influence of other significant
23 sources on ambient mixing ratios of C₃ alkyl nitrates at TW.

24 **3.2.2. Source apportionment of alkyl nitrates**

25 Figure 7 presents the explained variations of species (as a percentage of the species
26 total) in the identified sources extracted by the PMF model. The standard errors in the
27 figure were obtained from a bootstrap analysis of the PMF model simulation. Since
28 the air masses arriving at TMS were photochemically aged (Guo et al., 2013a), the
29 source signatures of alkyl nitrates and their parent hydrocarbons were damaged at this
30 mountain site. Therefore, only the data collected at the urban site were used for source

1 apportionments of alkyl nitrates.
 2 High concentrations of O_x and alkyl nitrates were found in the first factor at both sites,
 3 implying that this factor was associated with secondary formation. In addition, certain
 4 amounts of combustion species, such as ethane, ethyne, propane, *n/i*-butanes, benzene
 5 and CO were present in this factor. It is not surprising that O_x correlated with the
 6 aforementioned species given that O₃ is a secondary pollutant formed from
 7 photochemical oxidation of RH (Ling and Guo, 2014). The second factor was
 8 distinguished by a significant presence of methyl chloride, ethene, ethyne and
 9 benzene along with certain amounts of methane, propane and *n/i*-butane. It is well
 10 established that methyl chloride, ethyne and benzene are typical tracers for biomass
 11 burning/biofuel combustion (Barletta et al., 2009; Guo et al., 2011). As biofuel was
 12 not in widespread use in Hong Kong (HKCSD, 2010), this factor was identified as
 13 biomass burning. The third factor was identified as oceanic emissions, as the tracer
 14 DMS had an exclusively high percentage in this source at both sites (Blake et al.,
 15 2003; Marandino et al., 2013). The last factor was dominated by high percentages of
 16 propane and *n/i*-butanes, typical tracers of liquefied petroleum gas (LPG). Therefore,
 17 this factor was identified as LPG usage.



18
 19 Figure 7. Explained variations of species in the identified sources extracted by the
 20 PMF model for TW.

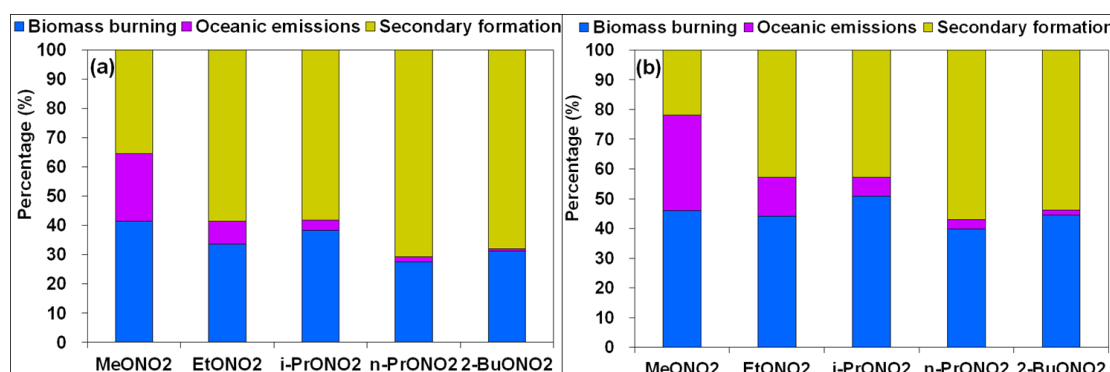
21

22 As mentioned earlier, regional transport and mesoscale circulation had a significant

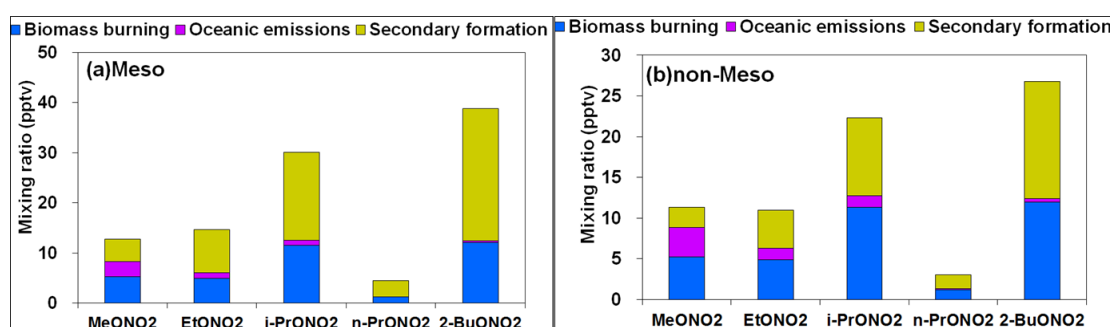
1 influence on the distribution of air pollutants at TMS and TW (Guo et al., 2012,
2 2013a). By using the Weather Research and Forecasting (WRF) model, air masses
3 affected by mesoscale circulation were distinguished from those affected by regional
4 transport (Guo et al., 2013a). Nine sampling days during the entire sampling period
5 (24, 29-31 October, 1-3, 9 and 19 November) were identified to be affected by
6 mountain-valley breezes (they were also O₃ episode days). Hence, we divided the
7 sampling period into two categories - “meso” and “non-meso” scenarios for source
8 apportionment analysis. The “meso” scenario included the nine O₃ episode days with
9 apparent mesoscale circulation, while the “non-meso” scenario covered the rest of the
10 sampling days.

11 By summing up the mass of the alkyl nitrates in each source, the total concentrations
12 of alkyl nitrates in each source were obtained and the contribution of each individual
13 source to alkyl nitrates at both sites was calculated. Figures 8 and 9 present the source
14 contributions to individual alkyl nitrates for the “meso” and “non-meso” scenarios in
15 percentage and in absolute concentration at TW, respectively. The mixing ratios of
16 total alkyl nitrates (*i.e.*, $\sum \text{RONO}_2 = \text{MeONO}_2 + \text{EtONO}_2 + 1\text{-PrONO}_2 + 2\text{-PrONO}_2 +$
17 2-BuONO_2) were higher in the “meso” scenario than those in “non-meso” scenario (p
18 < 0.05), with the average value of 100.9 ± 7.5 pptv for total alkyl nitrates in the “meso”
19 scenario, about 1.4 times those in the “non-meso” scenario. It was found that in the
20 “meso” scenario, secondary formation was the most significant contributor to the total
21 alkyl nitrate mixing ratios, with an average percentage of $60 \pm 2\%$ or absolute mixing
22 ratio of 60.2 ± 1.2 pptv, followed by biomass burning ($34 \pm 1\%$ or 35.1 ± 0.4 pptv)
23 and oceanic emissions ($6 \pm 1\%$ or 5.62 ± 0.06 pptv). On the other hand, in the
24 “non-meso” scenario the contributions of biomass burning ($46 \pm 2\%$ or 34.2 ± 0.7
25 pptv) and secondary formation ($44 \pm 2\%$ or 32.9 ± 0.7 pptv) were comparable, and the
26 oceanic emissions contributed $10 \pm 1\%$ or 7.0 ± 0.07 pptv to the total alkyl nitrates.
27 The higher contribution of secondary formation in the “meso” scenario at TW was
28 mainly due to stronger photochemical reactions. Indeed, the PBM-MCM model
29 simulation indicated that the average concentration of HO_x (HO_x = OH + HO₂) during
30 daytime hours (0700-1800 LT) in the “meso” scenario was $(2.5 \pm 0.7) \times 10^7$

1 molecule/cm³, about twice that of the “non-meso” scenario.



2
3 Figure 8. Source contributions to individual alkyl nitrates in (a) “meso” and (b)
4 “non-meso” scenarios at TW (in percentage).

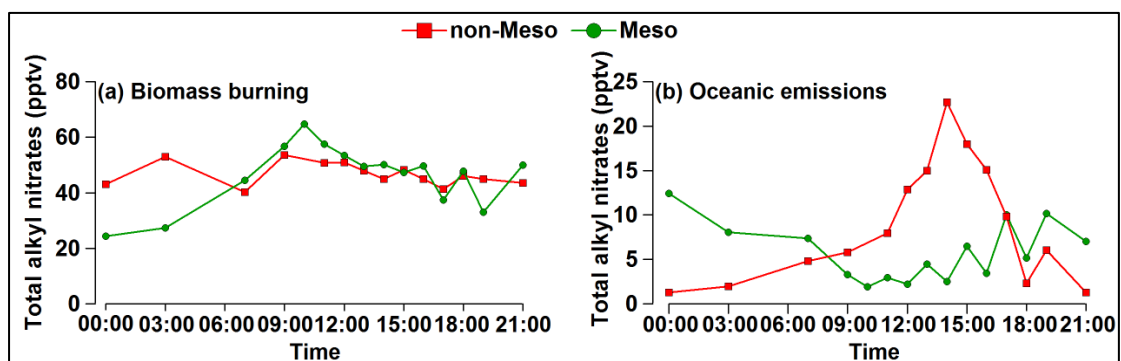


6
7 Figure 9. Source contributions to individual alkyl nitrates in (a) “meso” and (b)
8 “non-meso” scenarios at TW (in absolute concentration).

9
10 In addition, although the percentage contribution of biomass burning was higher in
11 the “non-meso” scenario, the absolute mixing ratios of biomass burning were
12 comparable in the two scenarios. Figure 10 shows the diurnal patterns of Σ RONO₂
13 from biomass burning and oceanic emissions in “meso” and “non-meso” scenarios at
14 TW. The contribution of biomass burning in the “meso” scenario was likely
15 attributable to the cooking/heating activities in the small villages nearby and the
16 frequent barbecue activities at the foot of the mountain (Guo et al., 2013a, b), as well
17 as the forest fire observed in the mountainous areas (AFCD, 2015). The regular
18 cooking/heating activities from 0700 to 1400 LT in many dim sum restaurants in the
19 village likely resulted in the increased levels of biomass burning in the morning until
20 noon. In contrast, the diurnal pattern in “non-meso” scenario was weak and the peaks
21 were not statistically different from the troughs. The difference of the average mixing
22 ratio of Σ RONO₂ between daytime and nighttime hours was only 1 pptv. The weak

1 diurnal variations in the “non-meso” scenario suggests that the contribution of fresh
 2 biomass burning was insignificant, revealing the influence of regional transport from
 3 the PRD region. This speculation was confirmed by the analysis of 12-h backward
 4 trajectories, which showed that air masses in the “non-meso” scenario were mainly
 5 from the inland PRD region (data not shown here). It is noteworthy that although air
 6 masses were more aged in the “non-meso” scenario, the levels of alkyl nitrates were
 7 comparable to those in the “meso” scenario, highlighting the strong emissions of
 8 biomass burning in the PRD region (Yuan et al., 2010).

9 For the oceanic emissions, a trough during daytime hours was found for ΣRONO_2 in
 10 the “meso” scenario, while a broad peak was present during daytime hours in the
 11 “non-meso” scenario. The daytime trough in the “meso” scenario at TW was related
 12 to uplifted valley breezes that brought alkyl nitrates away from TW to TMS, while the
 13 higher nighttime values were probably due to marine emissions and aged continental
 14 plumes which were re-circulated from the South China Sea to the coastal urban site at
 15 night. In contrast, the broad daytime peak in the “non-meso” scenario was likely
 16 associated with higher daytime temperature and solar radiation, leading to higher
 17 oceanic emissions that were transported from eastern China and southern China
 18 coastal regions to the TW site.



19
 20 Figure 10. Diurnal patterns of (a) biomass burning and (b) oceanic emissions for
 21 “meso” and “non-meso” scenarios at TW.

22
 23 Moreover, the contributions of oceanic emissions to C_1 - C_2 alkyl nitrates were higher
 24 than C_3 - C_4 alkyl nitrates, with average percentages of 23% and 32% for the “meso”
 25 and “non-meso” scenarios (Figures 8 and 9), suggesting the importance of oceanic
 26 emissions to C_1 - C_2 alkyl nitrates, consistent with the results of previous work

1 (Simpson et al., 2003). Instead, the C₃-C₄ alkyl nitrates were dominated by the
2 secondary formation in the “meso” scenario (58-71%), while the contributions of
3 biomass burning and secondary formation to C₃-C₄ alkyl nitrates were comparable in
4 the “non-meso” scenario.

5 6 **3.2.3. Contributions of mesoscale circulation, in-situ formation and regional** 7 **transport to alkyl nitrates at TMS**

8 Valley breezes brought freshly-emitted parent hydrocarbons and alkyl nitrates from
9 the urban areas at the foot of the mountain (TW) to the mountain summit (TMS)
10 during daytime hours, redistributing the ambient levels of alkyl nitrates at TMS (Guo
11 et al., 2013a; Lam et al., 2013). Indeed, except MeONO₂ which had comparable levels
12 in both “meso” and “non-meso” scenarios, the mixing ratios of daytime C₂-C₄ alkyl
13 nitrates were all higher in “meso” scenario than those in “non-meso” scenario ($p <$
14 0.05), with the average values of 14.21 ± 0.79 , 28.73 ± 1.70 , 4.67 ± 0.29 and 40.21 ± 2.79
15 pptv for EtONO₂, *i*-PrONO₂, *n*-PrONO₂ and 2-BuONO₂, respectively. To quantify the
16 influence of mesoscale circulation on the mixing ratios of alkyl nitrates at TMS, a
17 moving box model coupled with master chemical mechanism (Mbox) was applied to
18 the data collected on the days influenced by mesoscale circulation (*i.e.*, “meso”
19 scenario) (Guo et al., 2013a). The model was developed based on an idealized
20 trajectory movement between TMS and TW sites, with air pollutants transported from
21 TW to TMS through the valley breeze during daytime hours (0800-1700 LT) when
22 photochemical formation of alkyl nitrates was gradually undertaken, and eventually
23 contributed to the ambient alkyl nitrates at TMS. As such, the model was only
24 constrained with the observed daytime data at TW. On the other hand, the air masses
25 flew down the mountain due to the mountain breeze after sunset until the next
26 morning, and TMS was set as the center of the box model, which was constrained by
27 the data collected at TMS only for that period (Lam et al., 2013).

28 Table 3 presents the average concentrations of C₁-C₄ alkyl nitrates simulated by the
29 Mbox model at TMS, *i.e.*, the values under the “meso” scenario. It should be noted
30 that the comparison was only made for daytime alkyl nitrates (0800-1700LT), when
31 valley breeze occurred. The average mixing ratios of MeONO₂, EtONO₂, 1-PrONO₂,

1 2-PrONO₂ and 2-ButONO₂ at daytime hours estimated using the Mbox model were
2 9.97 ± 0.85, 7.38 ± 0.44, 3.08 ± 0.16, 18.7 ± 0.77 and 34.7 ± 3.14 pptv, respectively,
3 accounting for 86%, 52%, 66%, 65% and 86% of the observed values at TMS during
4 the same period, respectively, demonstrating that when there was mesoscale circulation,
5 the levels of alkyl nitrates at TMS were dominated by the photo-oxidation of their
6 parent hydrocarbons originated at TW, one possible reason leading to similar levels
7 of alkyl nitrates at the two sites though the values of their parent hydrocarbons were
8 lower at TMS.

9 For the “non-meso” scenario, the simulated levels of in-situ formation of MeONO₂,
10 EtONO₂, 1-PrONO₂, 2-PrONO₂ and 2-BuONO₂ at TMS were 3.61 ± 0.48, 2.18 ± 0.29,
11 1.03 ± 0.13, 3.68 ± 0.45 and 10.9 ± 1.31 pptv, respectively, accounting for 18-42% of
12 the observed C₁-C₄ alkyl nitrates, indicating that other sources rather than local
13 photochemical formation made significant contributions to ambient levels of alkyl
14 nitrates. As stated earlier, TMS was a mountain site with sparse anthropogenic
15 emissions nearby. However, the prevailing synoptic northerly winds in “non-meso”
16 scenario suggested possible regional sources of alkyl nitrates from inland PRD region
17 to the mountain site. Indeed, the impact of regional transport on the variations of air
18 pollutants at TMS for the days without mesoscale circulation, especially when the
19 prevailing winds were from the north with high speeds, was firmly confirmed in Guo
20 et al. (2013a). Hence, by excluding the locally-formed alkyl nitrates from the overall
21 levels of alkyl nitrates, we obtained the contribution of regional sources to alkyl
22 nitrates at TMS. The regional source contributions to MeONO₂, EtONO₂, 1-PrONO₂,
23 2-PrONO₂ and 2-BuONO₂ were 7.07 ± 0.50, 8.44 ± 0.62, 2.11 ± 0.22, 16.86 ± 1.17,
24 and 15.15 ± 1.49 pptv, respectively, accounting for 58-82% of the alkyl nitrates at
25 TMS. It is noteworthy that the regional alkyl nitrates included those photochemically
26 formed and emitted from biomass burning and oceanic sources in that the inland PRD
27 region.

28
29
30

1 Table 3. Mixing ratios of C₁-C₄ alkyl nitrates influenced by mesoscale circulation
 2 (“Meso”), in-situ formation and regional transport at TMS (unit: pptv).

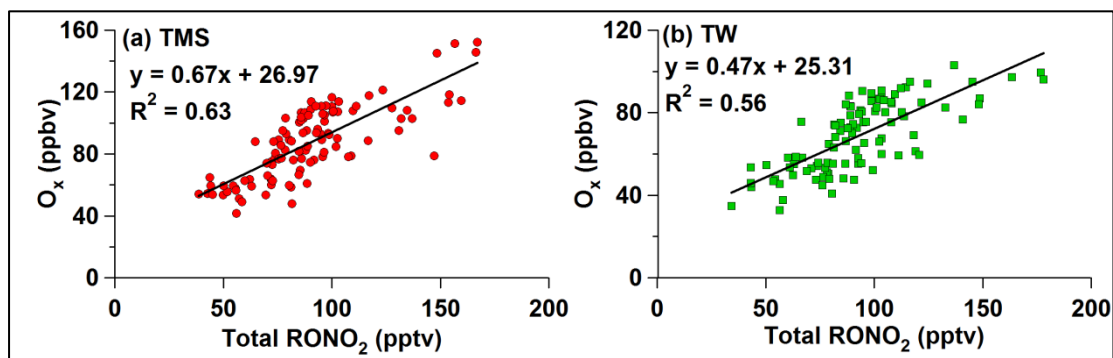
| Scenario | MeONO ₂ | EtONO ₂ | 1-PrONO ₂ | 2-PrONO ₂ | 2-BuONO ₂ |
|--------------------|--------------------|--------------------|----------------------|----------------------|----------------------|
| “Meso” | 9.97 ± 0.85 | 7.38 ± 0.44 | 3.08 ± 0.16 | 18.7 ± 0.77 | 34.7 ± 3.14 |
| In-situ formation | 3.61 ± 0.48 | 2.18 ± 0.29 | 1.03 ± 0.13 | 3.68 ± 0.45 | 10.9 ± 1.31 |
| Regional transport | 7.07 ± 0.50 | 8.44 ± 0.62 | 2.11 ± 0.22 | 16.86 ± 1.17 | 15.15 ± 1.49 |

3

4 **3.3. Relationship of alkyl nitrates with O₃**

5 Alkyl nitrates are mainly formed through the reaction of peroxy radical (RO₂) and NO.
 6 However, NO can be oxidized by RO₂ to form NO₂, which results in tropospheric O₃
 7 formation through NO₂ photolysis. Hence, investigating the relationship between
 8 alkyl nitrates and O₃ is of help to evaluate the influence of alkyl nitrates on O₃
 9 formation (Simpson et al., 2006). Since photochemical formation of O₃ and alkyl
 10 nitrates occurs during daytime hours, the relationship between O₃ and alkyl nitrates is
 11 usually evaluated using the observed daytime data (*i.e.*, 0900-1600 LT). In this study,
 12 the mixing ratios of O_x were used to recover the loss of O₃ due to the NO titration.
 13 Figure 11 shows the correlation between O_x and the total alkyl nitrates (ΣRONO₂) at
 14 daytime hours. Good correlations were found at TMS (R² = 0.63) and TW (R² = 0.56)
 15 with the slopes of 0.67 and 0.47 ppbv/pptv, respectively, suggesting that when 1 pptv
 16 of total alkyl nitrates were formed from the reaction of RO₂ and NO, 0.67 and 0.47
 17 ppbv of O_x could be simultaneously produced at TMS and TW, respectively. The
 18 relatively higher slope at TMS than at TW was owing to higher concentrations of HO_x
 19 radicals and higher photochemical reactivity of VOCs at TMS (Lyu et al., 2016). In
 20 addition, as the formation of alkyl nitrates consumes NO, it resulted in negative
 21 contribution to O₃ formation. To quantify the negative influence on O₃, the
 22 PBM-MCM model was applied to the whole data collected at TMS and TW,
 23 respectively (Lyu et al., 2016). It was obvious that the formation of alkyl nitrates
 24 made negative contributions to the O₃ production, with the average reduction of 64.6
 25 (TW: 24.9), 37.4 (11.0), 18.9 (2.6), 39.6 (11.1), and 115.1 (40.6) pptv of O₃ for the
 26 formation of MeONO₂, EtONO₂, 1-PrONO₂, 2-PrONO₂ and 2-BuONO₂ at TMS,

1 respectively. Furthermore, moderate to good correlation was found between the
2 simulated O₃ reduction and the photochemically formed alkyl nitrates at TMS (R² =
3 0.42) and TW (R² = 0.72), with the average O₃ reduction rate of -4.1 and -4.7
4 pptv/pptv, respectively. Namely, O₃ was reduced by 4.1 and 4.7 pptv if 1 pptv of alkyl
5 nitrates were formed at TMS and TW, respectively.



6
7 Figure 11. Correlation between O_x (O₃ + NO₂) and total alkyl nitrates at (a) TMS and
8 (b) TW.

9
10 Moreover, because secondary alkyl nitrates are formed through two main reaction
11 pathways, *i.e.*, “RO₂ + NO” and “RO + NO₂”, it is of interest to investigate the
12 relative contribution of the above pathways to the formation of alkyl nitrates. Two
13 scenarios for model simulation were run and compared. The first scenario was the
14 base case in which the model was run with all reaction pathways opened, while the
15 second scenario was the constrained case in which the pathway of RO₂ + NO →
16 RONO₂ was shut down. It was found that the reaction of “RO₂ + NO” was the
17 prominent pathway for the secondary formation of alkyl nitrates at the two sites. The
18 contributions of CH₃O₂ + NO to MeONO₂ accounted for about 72% and 50% of the
19 secondarily formed MeONO₂, while the contributions of RO₂ + NO were 97-99 and
20 95-99% of the secondarily formed C₂-C₄ alkyl nitrates at TMS and TW, respectively.
21 The results are similar to the findings obtained at Tai O, Hong Kong (Lyu et al., 2015).
22 The lower contributions of RO₂ + NO to MeONO₂ at the two sites were related to the
23 higher levels of CH₃O from the oxidation of CH₄ and the decomposition of larger RO₂
24 radicals.

25
26

1 **4. Conclusions**

2 Intensive field measurements of alkyl nitrates and their parent hydrocarbons were
3 conducted concurrently at a mountain site (TMS) and an urban site (TW) at the foot
4 of the same mountain in Hong Kong from September to November 2010. The levels
5 of MeONO₂, EtONO₂ and 2-PrONO₂ were slightly higher at TW than at TMS ($p <$
6 0.05), while the average mixing ratios of 1-PrONO₂ and 2-BuONO₂ were comparable
7 at the two sites ($p > 0.05$). However, the levels of the parent hydrocarbons of alkyl
8 nitrates were lower at TMS, implying the complexity of sources of alkyl nitrates.
9 Receptor model and photochemical box model simulations found that mesoscale
10 circulation and regional transport had a remarkable impact on the levels of alkyl
11 nitrates at the two sites. At TW, secondary formation was the dominant contributor to
12 alkyl nitrates when there was mesoscale circulation, while the contributions of
13 secondary formation and biomass burning were comparable under the influence of
14 regional transport. At TMS, on the days with mesoscale circulations the
15 photo-oxidation of parent hydrocarbons from TW accounted for 52-85% of the alkyl
16 nitrates at TMS, while on the days with regional impact, alkyl nitrates from the inland
17 PRD region were the major contributor to alkyl nitrate levels at TMS, with a
18 percentage contributions of 58-82%. The photo-oxidation of parent hydrocarbons
19 from TW and regional transport led to the similar values of alkyl nitrates observed at
20 the two sites. With regard to the secondarily formed alkyl nitrates, the reaction of RO₂
21 and NO was the prominent pathway at both sites. Moreover, the formation of alkyl
22 nitrates made negative contributions to the O₃ formation, with a reduction rate of -4.1
23 and -4.7 pptv O₃ per pptv alkyl nitrates at TMS and TW, respectively. The findings of
24 this study are expected to advance the understanding on the source contributions and
25 photochemical formation pathways of alkyl nitrates in mountainous areas in Hong
26 Kong.

27 28 **Acknowledgements**

29 This project was supported by the Research Grants Council of the Hong Kong Special
30 Administrative Region via grants PolyU5154/13E, PolyU152052/14E and

1 CRF/C5022-14G. This study was partly supported by the internal grants of the Hong
2 Kong Polytechnic University (4-BCAV and 1-ZVCX), and the National Natural
3 Science Foundation of China (No. 41405112 and 41275122). The challenging but
4 ultimately very helpful comments of the anonymous reviewers are greatly
5 appreciated.

6

7 **References**

8 AFCD (Agriculture, Fisheries and Conservation Department), 2008. Available at website:
9 <http://www.afcd.gov.hk/>.

10 AFCD (Agriculture, Fisheries and Conservation Department), useful statistics, Last Review Date
11 02 June 2015. Available at website: [http://www.afcd.gov.hk/english/country/cou_lea/
12 cou_lea_use/cou_lea_use.html](http://www.afcd.gov.hk/english/country/cou_lea/cou_lea_use/cou_lea_use.html).

13 Archibald, A.T., Khan, M.A.H., Watson, L.A., Utembe, S.R., Shallcross, D.E., Clemitshaw, K.C.,
14 Jenkin, M.E., 2007. Comment on 'Long-term atmospheric measurements of C₁-C₅ alkyl
15 nitrates in the Pearl River Delta region of southeast China' by Simpson et al. *Atmospheric
16 Environment* 41, 7369-7370.

17 Arey, J., Aschmann, S.M., Kwok, E.S.C., Atkinson, R., 2001. Alkyl nitrate, hydroxyl nitrate, and
18 hydroxycarbonyl formation from the NO_x-air photooxidations of C₅-C₈ n-alkanes. *Journal
19 of Physical Chemistry* 105, 1020-1027.

20 Atkinson, R., Baulch, D.L., Cox, R.A., Crowley, J.N., Hampson, R.F., Hynes, R.G., Jenkin, M.E.,
21 Rossi, M.J., Troe, J., Subcommittee, I., 2006. Evaluated kinetic and photochemical data for
22 atmospheric chemistry: volume II – gas phase reactions of organic species. *Atmospheric
23 Chemistry and Physics* 6, 3625-4055.

24 Barletta, B., Meinardi, S., Simpson, I.J., Atlas, E.L., Beyersdorf, A.J., Baker, A.K., Blake, N.J.,
25 Yang, M., Midyett, J.R., Novak, B.J., Mckeachie, R.J., Fuelberg, H.E., Sachse, G.W., Avery,
26 M.A., Campos, T., Weinheimer, A.J., Rowland, F.S., Blake, D.R., 2009. Characterization of
27 volatile organic compounds (VOCs) in Asian and north American pollution plumes during
28 INTEX-B: identification of specific Chinese air mass tracers. *Atmospheric Chemistry and
29 Physics* 9, 5371-5388.

30 Barletta, B., Meinardi, S., Simpson, I.J., Khwaja, H.A., Blake, D.R., Rowland, F.S., 2002. Mixing
31 ratios of volatile organic compounds (VOCs) in the atmosphere of Karachi, Pakistan.
32 *Atmospheric Environment* 36, 3429-3443.

33 Bertman, S.B., Roberts, J.M., Parrish, D.D., Buhr, M.P., Goldan, P.D., Kuster, W.C., Fehsenfeld,
34 F.C., Montzka, S.A., Westberg, H., 1995. Evolution of alkyl nitrates with air mass age.
35 *Journal of Geophysical Research* 100, 22805-22813.

36 Blake, N.J., D. R. Blake, A. L. Swanson, E. Atlas, F. Flocke, and F. S. Rowland, 2003. Latitudinal,

1 vertical, and seasonal variations of C1–C4 alkyl nitrates in the troposphere over the Pacific
2 Ocean during PEM-Tropics A and B: Oceanic and continental sources, *Journal of*
3 *Geophysical Research* 108(D2), 8242, doi:10.1029/2001JD001444, 2003.

4 Clemitshaw, K.C., Williams, J., Rattigan, O.V., Shallcross, D.E., Law, K.S., Cox, R.A., 1997.
5 Gas-phase ultraviolet absorption cross-sections and atmospheric lifetimes of several C2–C5
6 alkyl nitrates. *Journal of Photochemistry and Photobiology A: Chemistry* 102, 117–126.

7 Environmental Protection Agency (EPA), 2008. EPA Positive Matrix Factorization (PMF) 3.0
8 fundamentals and user guide.

9 Friend, A.J., Ayoko, G.A., Stelcer, E., Cohen, D., 2011. Source apportionment of PM_{2.5} at two
10 receptor sites in Brisbane, Australia. *Environmental Chemistry* 8, 569-580.

11 Gao, J., Wang, T., Ding, A.J., Liu, C.B., 2005. Observation study of ozone and carbon monoxide
12 at the summit of mount Tai (1534 m a.s.l.) in central-eastern China. *Atmospheric*
13 *Environment* 39, 4779-4791.

14 Guo, H., Jiang, F., Cheng, H.R., Simpson, I.J., Wang, X.M., Ding, A.J., Wang, T.J., Saunders, S.M.,
15 Wang, T., Lam, S.H.M., Blake, D.R., Zhang, Y.L., Xie, M., 2009. Concurrent observations of
16 air pollutants at two sites in the Pearl River Delta and the implication of regional transport.
17 *Atmospheric Chemistry and Physics* 9, 7343-7360.

18 Guo, H., Ling, Z.H., Cheung, K., Jiang, F., Wang, D.W., Simpson, I.J., Barletta, B., Meinardi, S.,
19 Wang, T.J., Wang, X.M., Saunders, S.M., Blake, D.R., 2013a. Characterization of
20 photochemical pollution at different elevations in mountainous areas in Hong Kong.
21 *Atmospheric Chemistry and Physics* 13, 3881-3898.

22 Guo, H., Ling, Z.H., Cheung, K., Wang, D.W., Simpson, I.J., Blake, D.R., 2013b. Acetone in the
23 atmosphere of Hong Kong: Abundance, sources and photochemical precursors. *Atmospheric*
24 *Environment* 65, 80-88.

25 Guo, H., Ling, Z.H., Simpson, I.J., Blake, D.R., Wang, D.W., 2012. Observations of isoprene,
26 methacrolein (MAC) and methyl vinyl ketone (MVK) at a mountain site in Hong Kong.
27 *Journal of Geophysical Research* 117, doi:10.1029/2012JD017750.

28 HKCSD (Hong Kong Census and Statistics Department), 2010. Hong Kong Energy Statistics:
29 Annual Report. <http://www.censtatd.gov.hk>.

30 HKEPD (Hong Kong Protection Department), 2012. Air Quality in Hong Kong.
31 2011. <http://www.epd-asg.gov.hk/english/report/aqr.html>.

32 Jenkin, M. E., Saunders, S. M., Wagner, V., and Pilling, M. J., 1997. The tropospheric degradation
33 of volatile organic compounds: A protocol for mechanism development. *Atmospheric*
34 *Environment* 31, 81-107, 1997.

35 Jenkin, M. E., Saunders, S. M., Wagner, V., and Pilling, M. J., 2003. Protocol for the development
36 of the master chemical mechanism MCMv3 (Part B): Tropospheric degradation of aromatic
37 volatile organic compounds, *Atmospheric Chemistry and Physics* 3, 181-193, 2003.

38 Jenkin, M.E., Clemitshaw, C., 2000. Ozone and other secondary photochemical pollutants:
39 Chemical processes governing their formation in the planetary boundary layer. *Atmospheric*

1 Environment 34, 2499-2527.

2 Jiang, F., Guo, H., Wang, T.J., Cheng, H.R., Wang, X.M., Simpson, I.J., Ding, A.J., Saunders, S.M.,
3 Lam, S.H.M., Blake, D.R., 2010. An O₃ episode in the Pearl River Delta: field observation
4 and model simulation. *Journal of Geophysical Research* 115, doi:/10.1029/2009JD013583.

5 Kwok, E.S.C. and Atkinson, R., 1995. Estimation of hydroxyl radical reaction-rate constants for
6 gas-phase organic-compounds using a structure-reactivity relationship-an update.
7 *Atmospheric Environment* 29, 1685-1695.

8 Lam, S.H.M., Saunders, S.M., Guo, H., Ling, Z.H., Jiang, F., Wang, X.M., Wang, T.J., 2013.
9 Modelling VOC source impacts on high ozone episode days observed at a mountain summit
10 in Hong Kong under the influence of mountain-valley breezes. *Atmospheric Environment* 81,
11 166-176.

12 Ling, Z.H. and Guo, H., 2014. Contribution of VOC sources to photochemical ozone formation
13 and its control policy implication in Hong Kong. *Environmental Science and Policy* 38,
14 180-191.

15 Ling, Z.H., Guo, H., Cheng, H.R., Yu, Y.F., 2011. Sources of ambient volatile organic compounds
16 and their contributions to photochemical ozone formation at a site in the Pearl River Delta,
17 southern China. *Environmental Pollution* 159, 2310-2319.

18 Ling, Z.H., Guo, H., Lam, S.H.M., Saunders, S.M., Wang, T., 2014. Atmospheric photochemical
19 reactivity and ozone production at two sites in Hong Kong: Application of a Master Chemical
20 Mechanism-photochemical box model. *Journal of Geophysical Research* 119,
21 doi:10.1002/2014JD021794.

22 Lyu, X.P., Ling, Z.H., Guo, H., Zeng, L.W., Wang, N., 2016. Impact of alkyl nitrate chemistry on
23 photochemical reactivity and O₃ production in Hong Kong. In preparation.

24 Lyu, X.P., Ling, Z.H., Guo, H., Saunders, S.M., Lam, S.H.M., Wang, N., Wang, Y., Liu, M., Wang,
25 T., 2015. Re-examination of C₁-C₅ alkyl nitrates in Hong Kong using an observation-based
26 model. *Atmospheric Environment* 120, 28-37.

27 Marandino, C.A., Tegtmeier, S., Krüger, K., Zindler, C., Atlas, E.L., Moore, F., Bange, H.W., 2013.
28 Dimethylsulphide (DMS) emissions from the western Pacific Ocean: a potential marine
29 source for stratospheric sulphur? *Atmospheric Chemistry and Physics* 13, 8427-8437.

30 Paatero, P., 2000. User's guide for Positive Matrix Factorization Programs PMF2 and PMF3, part
31 1: Tutorial. Prepared by University of Helsinki, Finland (February).

32 Pinho, P.G., Lemos, L.T., Pio, C.A., Evtuygina, M.G., Nunes, T.V., Jenkin, M.E., 2009. Detailed
33 chemical analysis of regional-scale air pollution in western Portugal using an adapted version
34 of MCM v3.1. *Science of the Total Environment* 407, 2024-2038.

35 Reeves, C.E., Slemr, J., Oram, D.E., Worton, D., Penkett, S.A., Stewart, D.J., Purvis, R., Watson,
36 N., Hopkins, J., Lewis, A., Methven, J., Blake, D.R., Atlas, E., 2007. Alkyl nitrates in outflow
37 from North America over the North Atlantic during intercontinental transport of ozone and
38 precursors 2004. *Journal of Geophysical Research* 112, D10S037, doi:
39 10.1029/2006JD007567.

1 Roberts, J.M., Bertman, S.B., Parrish, D.D., Fehsenfeld, F.C., Johnson, B.T., Niki, H., 1998.
2 Measurements of alkyl nitrates at Chebogue Point Nova Scotia during the 1993 North
3 Atlantic Regional Experiment (NARE) intensive. *Journal of Geophysical Research* 103 (D11),
4 13569-13580.

5 Russo, R.S., Zhou, Y., Haase, K.B., Wingenter, O.W., Frinak, E.K., Mao, H., Talbot, R.W., Sive,
6 B.C., 2010. Temporal variability, sources and sinks of C₁-C₅ alkyl nitrates in coastal New
7 England. *Atmospheric Chemistry and Physics* 10, 1865-1883.

8 Saunders, S. M., Jenkin, M. E., Derwent, R. G., and Pilling, M. J., 2003. Protocol for the
9 development of the master chemical mechanism MCMv3 (Part A): Tropospheric degradation
10 of non-aromatic volatile organic compounds. *Atmospheric Chemistry and Physics* 3,
11 161-180.

12 Seinfeld, J.H. and Pandis, S.N., 2006. *Atmospheric Chemistry and Physics: from air pollution to*
13 *climate change*, 2nd edition. Wiley Publisher, New Jersey, USA.

14 Simpson, I.J., Akagi, S.K., Barletta, B., Blake, N.J., Choi, Y., Diskin, G.S., Fried, A., Fuelberg,
15 H.E., Meinardi, S., Rowland, F.S., Vay, S.A., Weinheimer, A.J., Wennberg, P.O., Wiebring, P.,
16 Wisthaler, A., Yang, M., Yokelson, R.J., Blake, D.R., 2011. Boreal forest fire emissions in
17 fresh Canadian smoke plumes: C₁-C₁₀ volatile organic compounds (VOCs), CO₂, CO, NO₂,
18 NO, HCN and CH₃CN. *Atmospheric Chemistry and Physics* 11, 6445–6463.

19 Simpson, I.J., Blake, N.J., Barletta, B., Diskin, G.S., Fuelberg, H.E., Gorham, K., Huey, L.G.,
20 Meinardi, S., Rowland, F.S., Vay, S.A., Weinheimer, A.J., Yang, M., Blake, D.R., 2010.
21 Characterization of trace gases measured over Alberta oil sands mining operations: 76
22 speciated C₂-C₁₀ volatile organic compounds (VOCs), CO₂, CH₄, CO, NO, NO₂, NO_y, O₃ and
23 SO₂. *Atmospheric Chemistry and Physics* 10, 11931-11954.

24 Simpson, I.J., Blake, N.J., Blake, D.R., Atlas, E., Flocke, F., Crawford, J.H., Fuelberg, H.E., Kiley,
25 C.M., Meinardi, S., Rowland, F.S., 2003. Photochemical production and evolution of selected
26 C₂-C₅ alkyl nitrates in tropospheric air influenced by Asia outflow. *Journal of Geophysical*
27 *Research* 108, D20, doi:10.1029/2002JD002830.

28 Simpson, I.J., Meinardi, S., Blake, D.R., Blake, N.J., 2002. A biomass burning source of C₁-C₄
29 alkyl nitrates. *Geophysical Research Letters* 29 (24), 2168, doi: 10.1029/2002GL016290.

30 Simpson, I.J., Wang, T., Guo, H., Kwok, Y.H., Flocke, F., Atlas, E., Meinardi, S., Rowland, F.S.,
31 Blake, D.R., 2006. Long-term atmospheric measurements of C₁-C₅ alkyl nitrates in the Pearl
32 River Delta region of southeast China. *Atmospheric Environment* 40, 1619-1632.

33 Sommariva, R., Trainer, M., de Gouw, J.A., Roberts, J.M., Warneke, C., Atlas, E., Flocke, F.,
34 Goldan, P.D., Kuster, W.C., Swanson, A.L., Fehsenfeld, F.C., 2008. A study of organic
35 nitrates formation in an urban plume using a Master Chemical Mechanism. *Atmospheric*
36 *Environment* 42, 5771-5786.

37 Talukdar, R.K., Burkholder, J.B., Hunter, M., Gilles, M.K., Roberts, J.M., Ravishankara, A.R.,
38 1997. Atmospheric fate of several alkyl nitrates Part 2 UV absorption cross-sections and
39 photodissociation quantum yields. *Journal of the Chemical Society, Faraday Transactions* 93,

1 2797–2805.

2 Wang, M., Shao, M., Chen, W.T., Lu, S.H., Wang, C., Huang, D.K., Yuan, B., Zeng, L.M., Zhao,
3 Y., 2013. Measurements of C₁-C₄ alkyl nitrates and their relationships with carbonyl
4 compounds and O₃ in Chinese cities. *Atmospheric Environment* 81, 389-398.

5 Wang, T., Poon, C.N., Kwok, Y.H., Li, Y.S., 2003. Characterizing the temporal variability and
6 emission patterns of pollution plumes in the Pearl River Delta of China. *Atmospheric*
7 *Environment* 37, 3539-3550.

8 Wang, T., Wong, H.L.A., Tang, J., Ding, A., Wu, W.S., Zhang, X.C., 2006. On the origin of surface
9 ozone and reactive nitrogen observed at a remote site in the northeastern Qinghai-Tibetan
10 Plateau, western China. *Journal of Geophysical Research* 111, D08303, doi:
11 10.1029/2005JD006527.

12 Worton, D.R., Reeves, C.E., Penkett, S.A., Sturges, W.T., Slemr, J., Oram, D.E., Bandy, B.J.,
13 Bloss, W.J., Carslaw, N., Davey, J., Emmerson, K.M., Gravestock, T.J., Hamilton, J.F., Heard,
14 D.E., Hopkins, J.R., Hulse, A., Ingram, T., Jacob, M.J., Lee, J.D., Leigh, R.J., Lewis, A.C.,
15 Monks, P.S., Smith, S.C., 2010. Alkyl nitrate photochemistry during the tropospheric organic
16 chemistry experiment. *Atmospheric Environment* 44, 773-785.

17 Wu, Z.Y., Wang, X.M., Chen, F., Turnipseed, A.A., Guenther, A., Niyogi, D., Charusombat, U.,
18 Xia, B.C., Munger, J.W., Alapty, K., 2011. Evaluating the calculated dry deposition velocities
19 of reactive nitrogen oxides and ozone from two community models over a temperate
20 deciduous forest. *Atmospheric Environment* 45, 2633-2674.

21 Yuan, B., Liu, Y., Shao, M., Lu, S.H., Streets, D.G., 2010. Biomass burning contributions to
22 ambient VOCs species at a receptor site in the Pearl River Delta (PRD), China.
23 *Environmental Science and Technology* 44, 4577-4582.

24

25

26